Supplemental Information for:

Structural Changes in 2-D BiSe Bilayers as n Increases in $(BiSe)_{1+\delta}(NbSe_2)_n$ (n = 1 - 4) Heterostructures

*Gavin Mitchson[1], Erik Hadland[1], Fabian Göhler[2], Martina Wanke[2], Marco Esters[1], Jeffrey Ditto[1], Erik Bigwood[1], Kim Ta[1], Richard G. Hennig[3], Thomas Seyller[2], and David C. Johnson[1]**

[1]Department of Chemistry

1253 University of Oregon

Eugene, OR 97401, USA

[2]Technische Universität Chemnitz

Institut für Physik

Professur für Technische Physik

Reichenhainer Strasse 70

D-09126 Chemnitz, Germany

[3]Department of Materials Science and Engineering

University of Florida

Gainesville, Florida 32611, USA

Table S1. Summary table of X-ray diffraction and composition measurements from samples with n = 1 - 4, including the off-stoichiometry compounds.

Sample	n	BiSe basal plane	BiSe *a* (nm)	BiSe *b* (nm)	$NbSe_2$ *a* (nm)	*c* (nm)	XRD Misfit	XRF Bi*n/Nb
1a	1	Rect.	4.45(2)	4.23(2)	3.47(1)	1.2081(1)	1.11(2)	1.12
2a	2	Square	4.24(2)	4.24(2)	3.47(1)	1.8447(1)	1.16(2)	1.14
2b	2	Rect.	4.40(3)	4.19(3)	3.467(3)	1.86(3)	1.13(2)	1.11
2c	2	Rect.	4.47(2)	4.22(2)	3.47(3)	1.858(2)	1.11(3)	0.95
3a	3	Square	4.24(1)	4.24(1)	3.47(1)	2.4682(2)	1.16(1)	1.13
3b	3	Rect.	4.46(3)	4.21(2)	3.46(2)	2.514(5)	1.10(3)	0.91
4a	4	Square	4.24(1)	4.24(1)	3.47(1)	3.1230(2)	1.16(1)	1.12

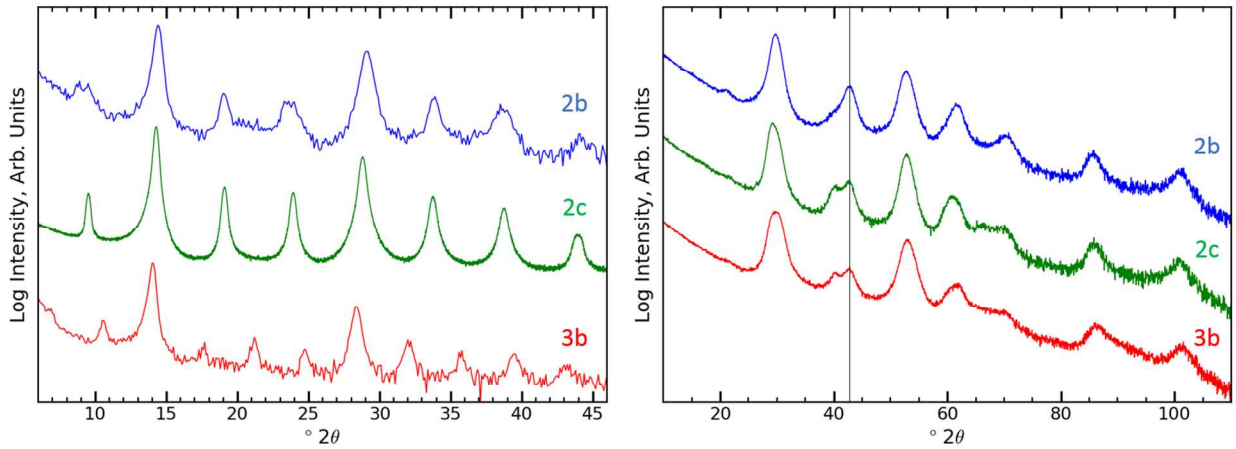

Figure S1. (left) 00*l* XRD scans for samples 2b and 2c (n = 2) and 3b (n = 3). (right) *hk0* XRD scans for the same samples. The black line at ~42 °2θ serves to highlight the shoulder present on left side of the BiSe (020) reflections for all three samples. Although all expected 00*l* reflections are present in these samples, some have weak intensities (2b and 3b) or misshapen peaks (2b). Hence although sample 2b has a measured Bi/Nb ratio similar to that of 2a, the weaker and somewhat misshaped XRD intensities suggest that the sample is not as well-formed. This could be due to the right ratio of Bi and Nb in the precursor, but too much absolute material in each

layer of the precursor to form the targeted compound (the overall film thickness of the sample measured using XRR was greater than that predicted based on the number of repeat units deposited in the precursor times the repeat unit thickness in the annealed sample). Interestingly, the *00l* scan for sample 2c suggests that despite a measured Bi/Nb ratio of only 0.95, this sample formed with a high degree of crystallographic alignment to the substrate. A similar observation is made for sample 3b, with a measured Bi/Nb ratio of only 0.91. All of these samples show a rectangular basal plane, instead of the square basal plane found in the higher quality or on-stoichiometry compounds. These observations suggest that the ratio of Bi/Nb in the film or the absolute amount of material within the precursor layers also influences the BiSe bilayer structure.

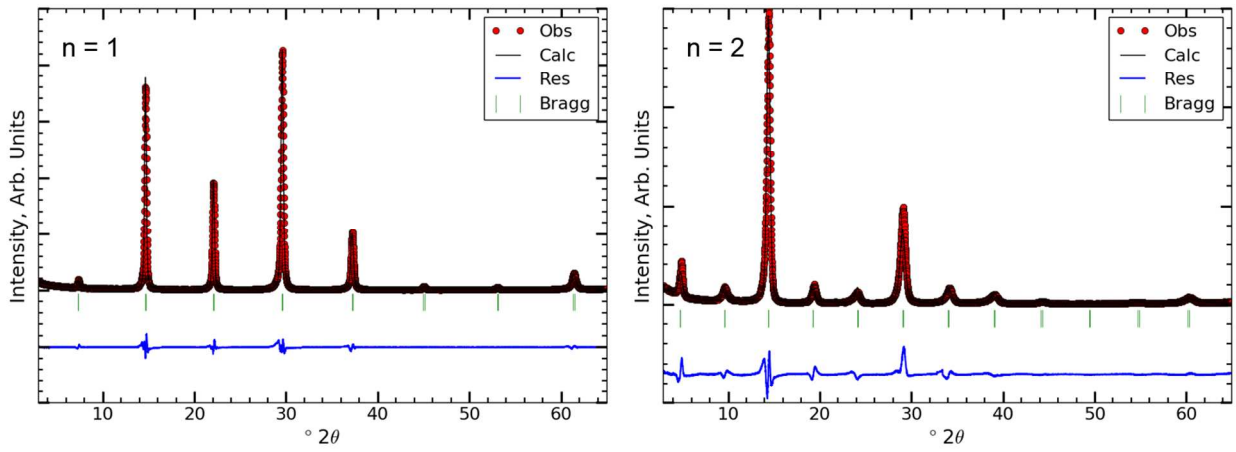

Figure S2. Comparison of observed XRD data (red circles) with refined model fit (black line) for the n = 1 and n = 2 samples. The blue trace plots the residuals of the model fit and the green vertical lines mark the locations of Bragg reflections.

Table S2. Rietveld refinement results from specular X-ray diffraction data for samples of $[(BiSe)_{1+\delta})_1(NbSe_2)_n$ with n = 1 and 2. The refinements were carried out using space group $P\bar{3}m1$.

n = 1		n = 2	
Composition from refinement	$[(BiSe)_{1.01}]_1(NbSe_2)_1$	Composition from refinement	$[(BiSe)_{0.99}]_1(NbSe_2)_2$
Composition from XRF	$[(BiSe)_{1.12}]_1(NbSe_2)_1$	Composition from XRF	$[(BiSe)_{1.14}]_1(NbSe_2)_2$
Radiation	Bruker D8, Cu K_α	Radiation	Bruker D8, Cu K_α
2θ range (degrees)	$3 \leq 2\theta \leq 65$	2θ range (degrees)	$3 \leq 2\theta \leq 65$
c (nm)	1.208(1)	*c* (nm)	1.8447(8)
Reflections in refinement	8	Reflections in refinement	12
Number of variables	12	Number of variables	15
$R_F = \Sigma \lvert F_o - F_c \rvert / \Sigma F_o$	0.0103	$R_F = \Sigma \lvert F_o - F_c \rvert / \Sigma F_o$	0.0325
$R_I = \Sigma \lvert I_o - I_c \rvert / \Sigma I_o$	0.0130	$R_I = \Sigma \lvert I_o - I_c \rvert / \Sigma I_o$	0.0598
$R_{wP} = [\Sigma w_i \lvert y_{oi} - y_{ci} \rvert^2 / \Sigma w_i \lvert y_{oi} \rvert^2]^{1/2}$	0.129	$R_{wP} = [\Sigma w_i \lvert y_{oi} - y_{ci} \rvert^2 / \Sigma w_i \lvert y_{oi} \rvert^2]^{1/2}$	0.235
$R_P = \Sigma \lvert y_{oi} - y_{ci} \rvert / \Sigma \lvert y_{oi} \rvert$	0.0844	$R_P = \Sigma \lvert y_{oi} - y_{ci} \rvert / \Sigma \lvert y_{oi} \rvert$	0.201
$R_e = [(N-P+C)/(\Sigma w_i y^2_{oi})]^{1/2}$	0.0452	$R_e = [(N-P+C)/(\Sigma w_i y^2_{oi})]^{1/2}$	0.0637
$\chi^2 = (R_{wP}/R_e)^2$	8.10	$\chi^2 = (R_{wP}/R_e)^2$	13.6
Atom parameters		**Atom parameters**	
Nb in 1a(0)		Se1 in 2*c* (*z*), *z*	0.0838(1)
Occ.	1.0	Occ.	2.0
Se1 in 2c (z), z	0.1346(1)	Nb1 in 2*c* (*z*), *z*	0.1715(1)
Occ.	2.0	Occ.	2.0
Bi in 2c (z), z	0.3757(3)	Se2 in 2*c* (*z*), *z*	0.2597(1)
Occ.	1.01(1)	Occ.	2.0
Se2 in 2c (z), z	0.3977(6)	Bi1 in 2*c* (*z*), *z*	0.4178(1)
Occ.	1.01(1)	Occ.	0.99(1)
		Se3 in 2*c* (z), z	0.4464(1)
		Occ.	0.99(1)

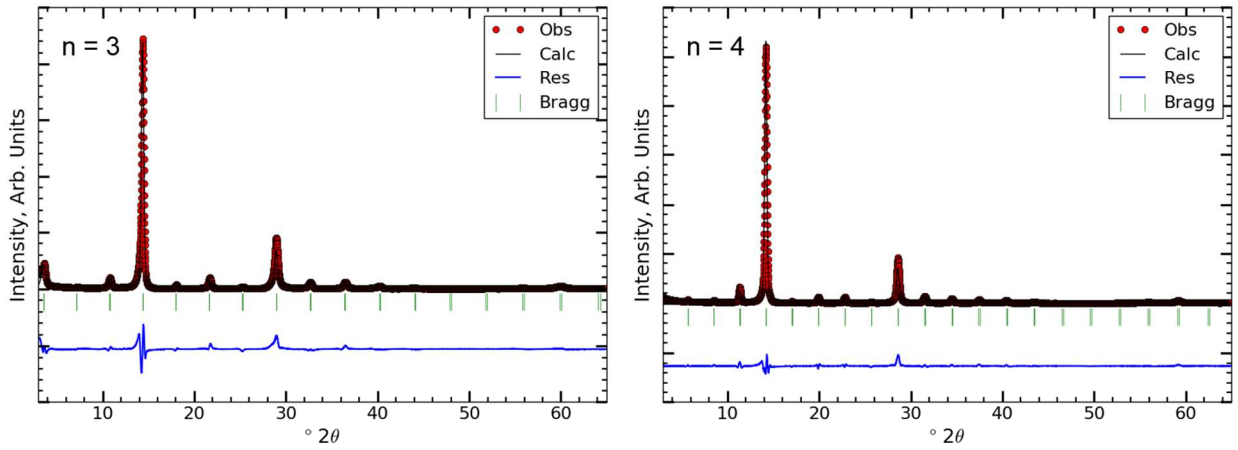

Figure S3. Comparison of observed XRD data (red circles) with refined model fit (black line) for the n = 3 and 4 samples. The blue trace plots the residuals of the model fit and the green vertical lines mark the locations of Bragg reflections.

Table S3. Rietveld refinement results from specular X-ray diffraction data for samples of $[(BiSe)_{1+\delta})_1(NbSe_2)_n$ with n = 3 and 4. The refinements were carried out using space group $P\bar{3}m1$.

n = 3		n = 4	
Composition from refinement	$[(BiSe)_{0.99}]_1(NbSe_2)_3$	Composition from refinement	$[(BiSe)_{1.03}]_1(NbSe_2)_4$
Composition from XRF	$[(BiSe)_{1.13}]_1(NbSe_2)_3$	Composition from XRF	$[(BiSe)_{1.12}]_1(NbSe_2)_4$
Radiation	Bruker D8, Cu K_α	Radiation	Bruker D8, Cu K_α
2θ range (degrees)	$3 \leq 2\theta \leq 65$	2θ range (degrees)	$3 \leq 2\theta \leq 65$
c (nm)	2.4683(4)	c (nm)	3.1231(6)
Reflections in refinement	17	Reflections in refinement	21
Number of variables	16	Number of variables	17
$R_F = \Sigma \lvert F_o - F_c \rvert / \Sigma F_o$	0.108	$R_F = \Sigma \lvert F_o - F_c \rvert / \Sigma F_o$	0.0778
$R_I = \Sigma \lvert I_o - I_c \rvert / \Sigma I_o$	0.114	$R_I = \Sigma \lvert I_o - I_c \rvert / \Sigma I_o$	0.0581
$R_{wP} = [\Sigma w_i \lvert y_{oi} - y_{ci} \rvert^2 / \Sigma w_i \lvert y_{oi} \rvert^2]^{1/2}$	0.297	$R_{wP} = [\Sigma w_i \lvert y_{oi} - y_{ci} \rvert^2 / \Sigma w_i \lvert y_{oi} \rvert^2]^{1/2}$	0.208
$R_P = \Sigma \lvert y_{oi} - y_{ci} \rvert / \Sigma \lvert y_{oi} \rvert$	0.237	$R_P = \Sigma \lvert y_{oi} - y_{ci} \rvert / \Sigma \lvert y_{oi} \rvert$	0.148
$R_e = [(N-P+C)/(\Sigma w_i y^2_{oi})]^{1/2}$	0.0468	$R_e = [(N-P+C)/(\Sigma w_i y^2_{oi})]^{1/2}$	0.0487
$\chi^2 = (R_{wP}/R_e)^2$	40.2	$\chi^2 = (R_{wP}/R_e)^2$	18.2
Atom parameters		**Atom parameters**	
Nb1 in 1*a*(0)		Se1 in 2*c* (*z*), *z*	0.0531(1)
Occ.	1.0	Occ.	2.0
Se1 in 2*c* (*z*), *z*	0.0652(1)	Nb1 in 2*c* (*z*), *z*	0.1051(1)
Occ.	2.0	Occ.	2.0
Se2 in 2*c* (*z*), *z*	0.1914(1)	Se2 in 2*c* (*z*), *z*	0.1559(1)
Occ.	2.0	Occ.	2.0
Nb2 in 2c(0)	0.2555(1)	Se3 in 2*c* (*z*), *z*	0.2540(1)
Occ.	1.0	Occ.	2.0
Se3 in 2*c* (*z*), *z*	0.3209(1)	Nb2 in 2*c* (*z*), *z*	0.3055(1)
Occ.	2.0	Occ.	2.0
Bi1 in 2*c* (*z*), *z*	0.4396(1)	Se4 in 2*c* (*z*), *z*	0.3586(1)
Occ.	0.99(1)	Occ.	2.0
Se4 in 2*c* (z), z	0.4606(1)	Bi in 2*c* (*z*), *z*	0.4520(1)
Occ.	0.99(1)	Occ.	1.03(1)
		Se5 in 2*c* (z), z	0.4684(1)
		Occ.	1.03(1)

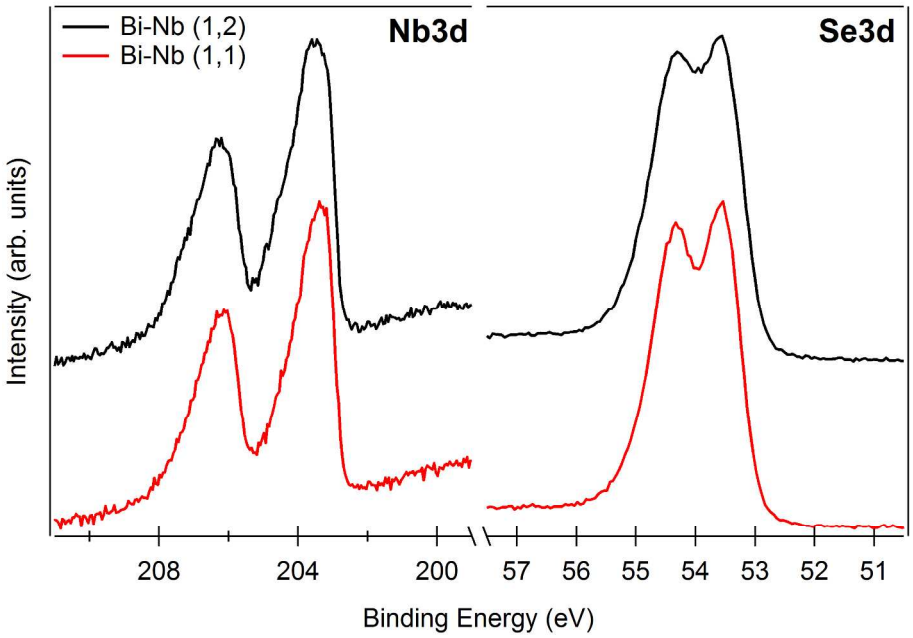

Figure S4. Core level XPS spectra for Nb 3d and Se 3d from the n = 1 (red) and n = 2 (black) compounds. The small changes in the peak shapes of the Se and Nb spectra be attributed to a change in the ratio of Se bound in $NbSe_2$ relative to Se bound in BiSe and a change of the environment of the $NbSe_2$ layers (no longer symmetrical).

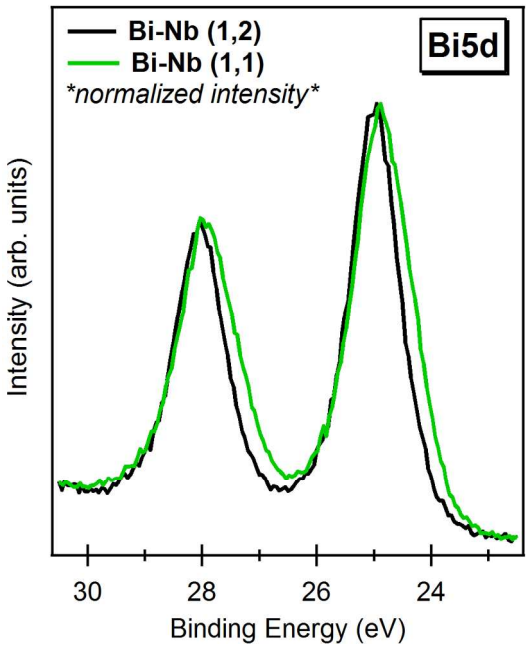

Figure S5. Overlaid Bi5d core level spectra of the n = 1 (bottom) and n = 2 (top) compounds. The high binding energy side of the peaks is the same, while the low binding energy side is broadened for the n = 1 compound relative to n = 2, indicating there is an additional component.

Table S4. Summary statistics for HAADF STEM image analysis from n > 1 compounds. "ABs" stands for antiphase boundaries. The [110] zone axis orientation is relative to an fcc lattice.

N = 2		Average:		22%	N = 3		Average:		15%	N = 4		Average:		5%
Image	# [110] grains with ABs	# [110] grains w/o ABs		% w/ ABs	Image	# [110] grains with ABs	# [110] grains w/o ABs		% w/ ABs	Image	# [110] grains with ABs	# [110] grains w/o ABs		% w/ ABs
21.40.02	1		2	0.333333	09.55.37	1		4	0.2	21.10.57	0		1	0
21.42.39	0		1	0	09.57.09	2		3	0.4	21.13.17	0		6	0
21.44.48	0		2	0	09.58.05	1		4	0.2	21.14.28	1		0	1
21.47.32	0		3	0	10.01.05	0		1	0	21.15.28	0		2	0
21.48.38	0		3	0	10.03.16_000	0		1	0	21.17.39	0		3	0
21.50.06	2		1	0.666667	10.03.16_001	0		3	0	21.19.23	0		3	0
21.51.58	0		1	0	10.03.16_003	1		4	0.2	21.20.22	0		5	0
21.56.14	1		0	1	10.03.16_005	0		2	0	21.23.32	0		3	0
21.57.07	1		0	1	10.08.23	1		2	0.333333	21.24.30	0		3	0
22.00.06	1		1	0.5	10.11.04	0		3	0	21.27.44	0		4	0
22.02.00	0		1	0	10.12.41	0		4	0	21.27.44	0		4	0
22.04.58	0		1	0	10.13.27	0		2	0	21.29.18	1		4	0.2
22.07.07	0		1	0						21.33.10	0		3	0
22.08.36	0		4	0										
Total:	6		21	0.22	Total:	6		33	0.15	Total:	2		41	0.047

The HAADF STEM images used in the analysis are included on the following pages. BiSe grains with the appropriate [110] zone axis orientation, relative to an fcc lattice, included in the analysis are marked with boxes: red boxes for grains without ABs, and green boxes for grains with ABs. For the grains that are determined to have ABs, a yellow arrow marks its approximate location in the grain. As determining AB presence can be somewhat subjective, the numbers presented in the table above represent only an approximation. We have attempted to include in the analysis only those grains that are close enough to the [110] zone axis such that ABs should be resolvable. The small grain sizes, potential artifacts from FIB preparation, and lamellae thickness also add to the uncertainty, as occasionally an amorphous surface layer or multiple grains are visible when moving through-focus on the microscope. When this is the case, we have excluded those grains from the analysis as their interpretation is complicated. The images are labeled in the format of "1,n", where n is the number of $NbSe_2$ layers in the *c*-axis repeating unit.

1,2: Image 21.40.02

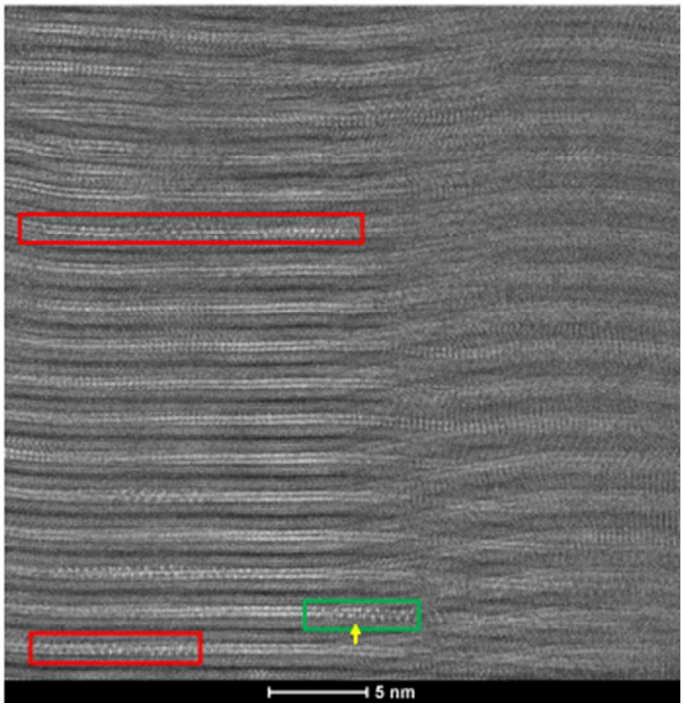

1,2: Image 21.42.39

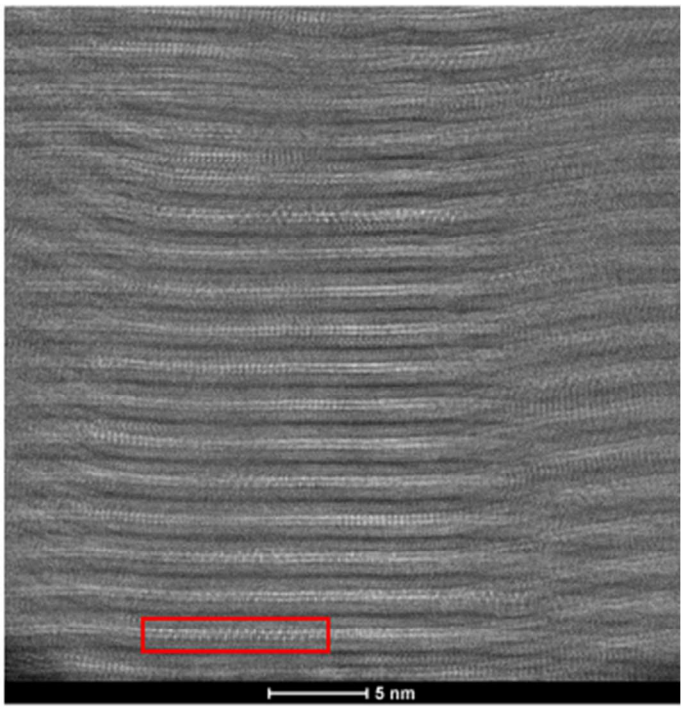

1,2: Image 21.44.48

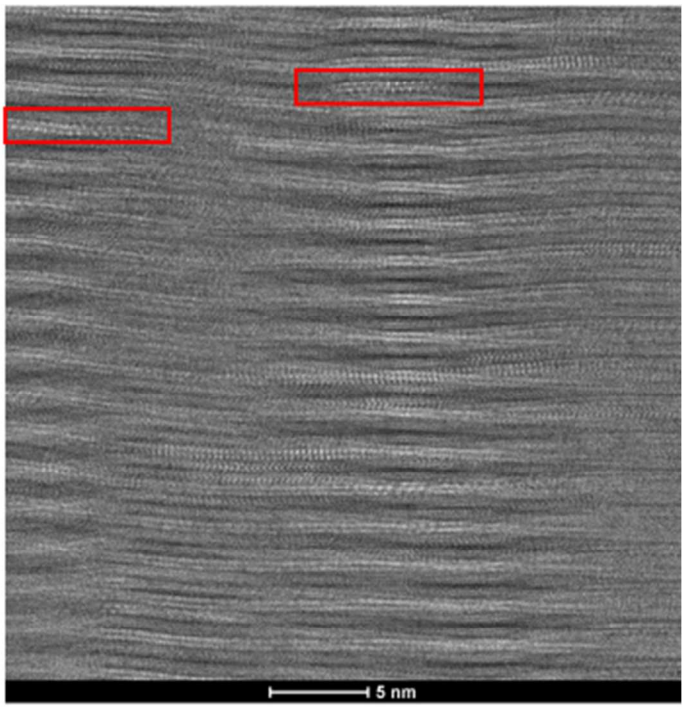

1,2: Image 21.47.32

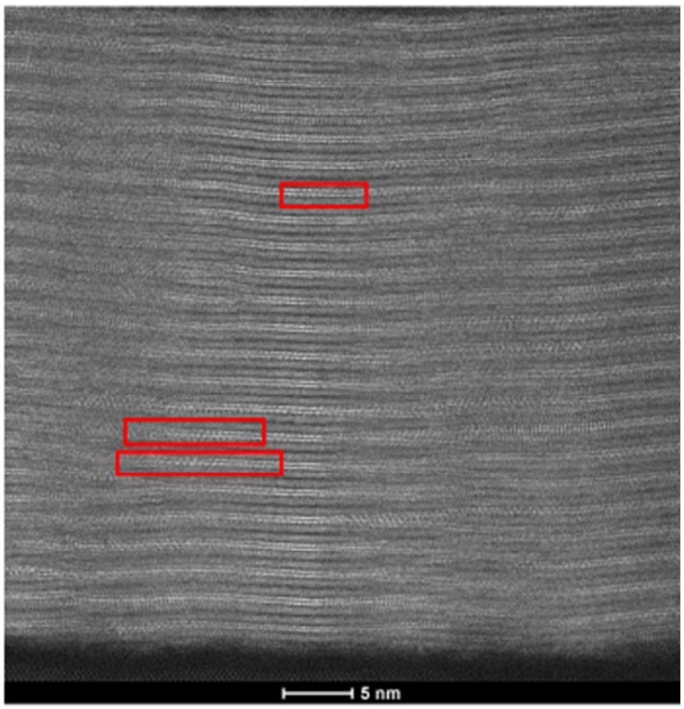

1,2: Image 21.48.38

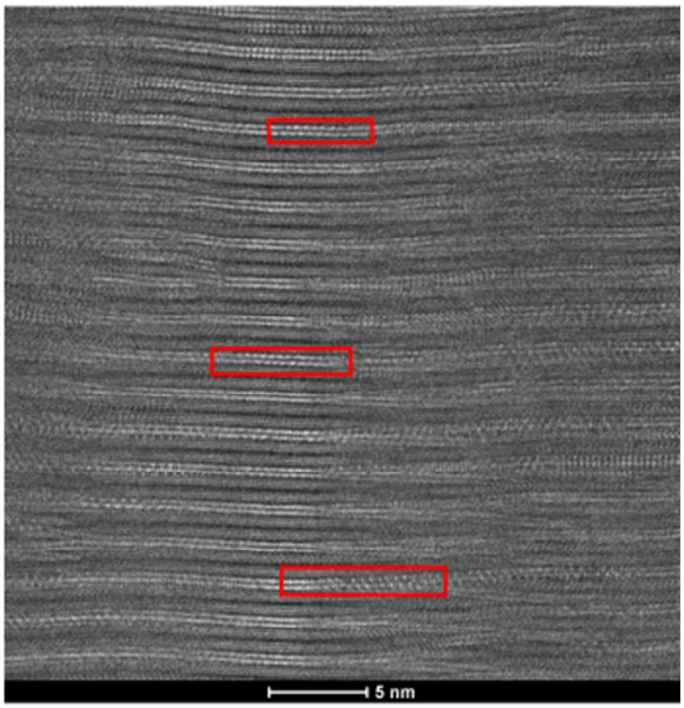

1,2: Image 21.50.06

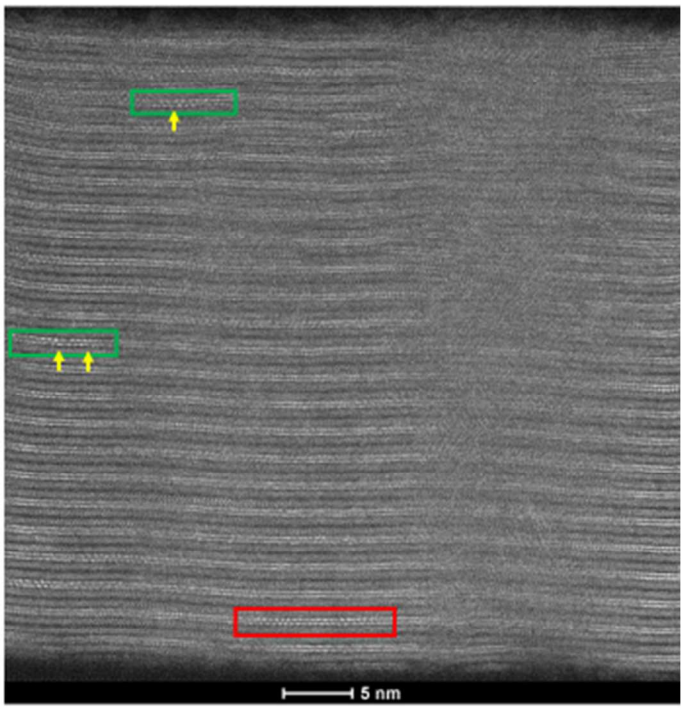

1,2: Image 21.51.58

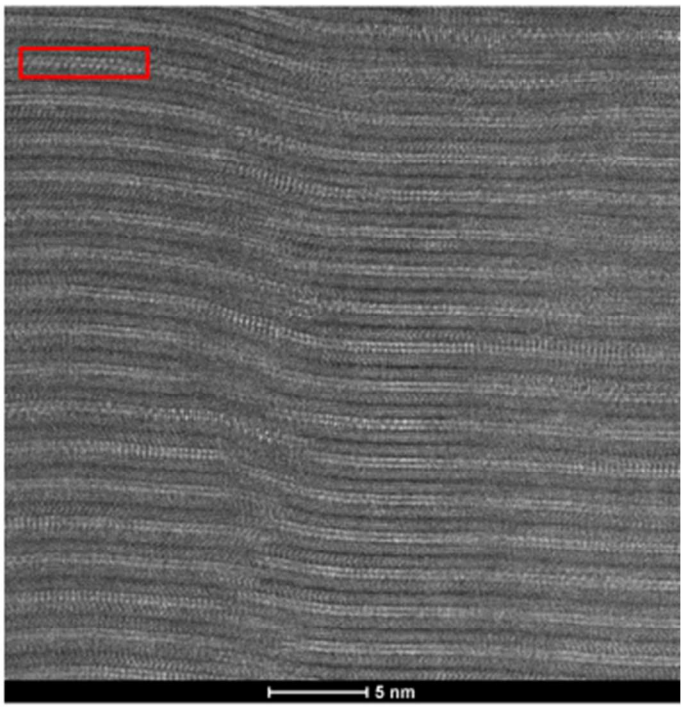

1,2: Image 21.56.14

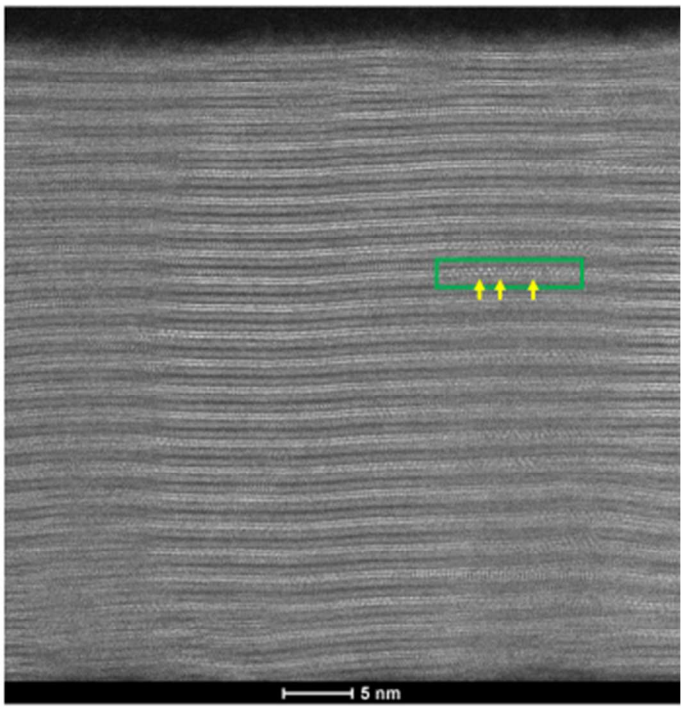

1,2: Image 21.57.07

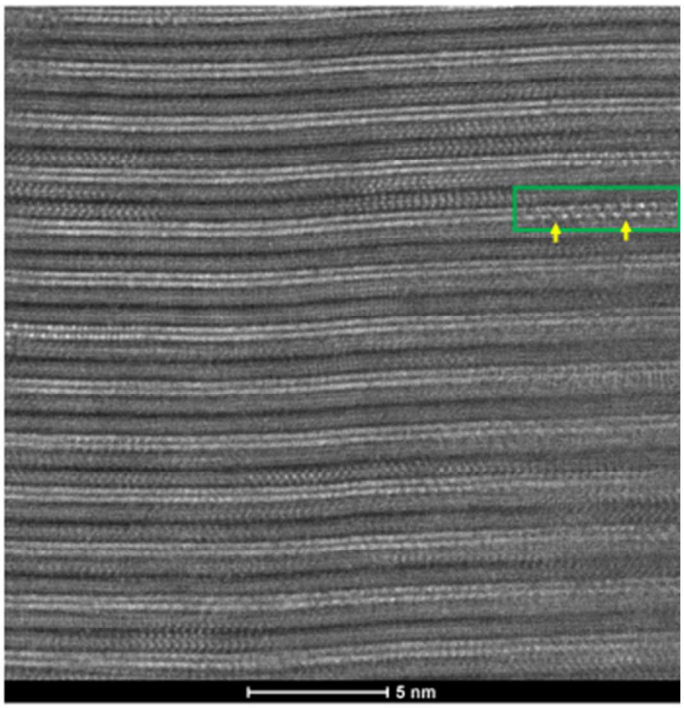

1,2: Image 22.00.06

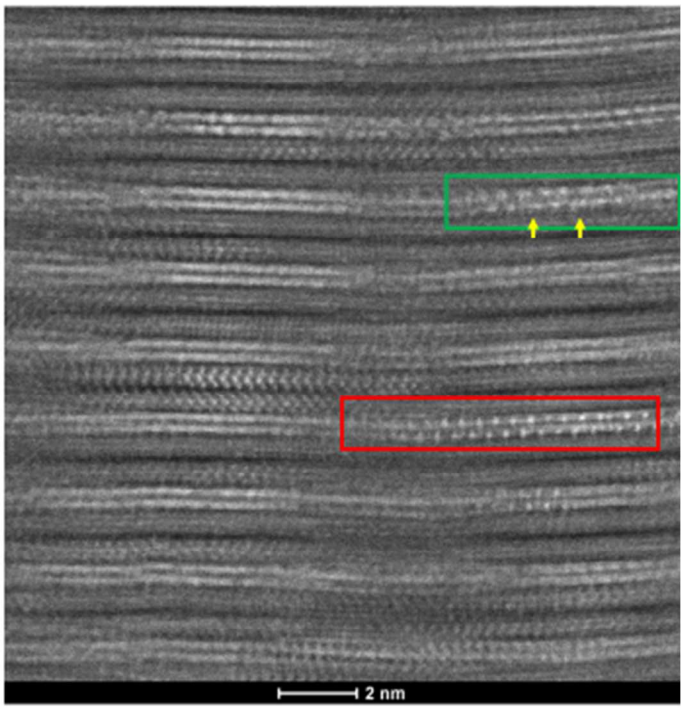

1,2: Image 22.02.00

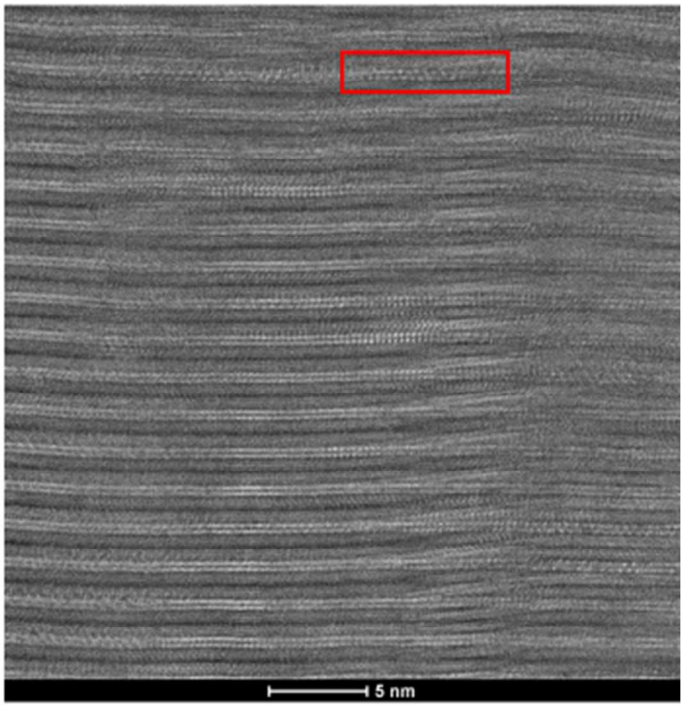

1,2: Image 22.02.00

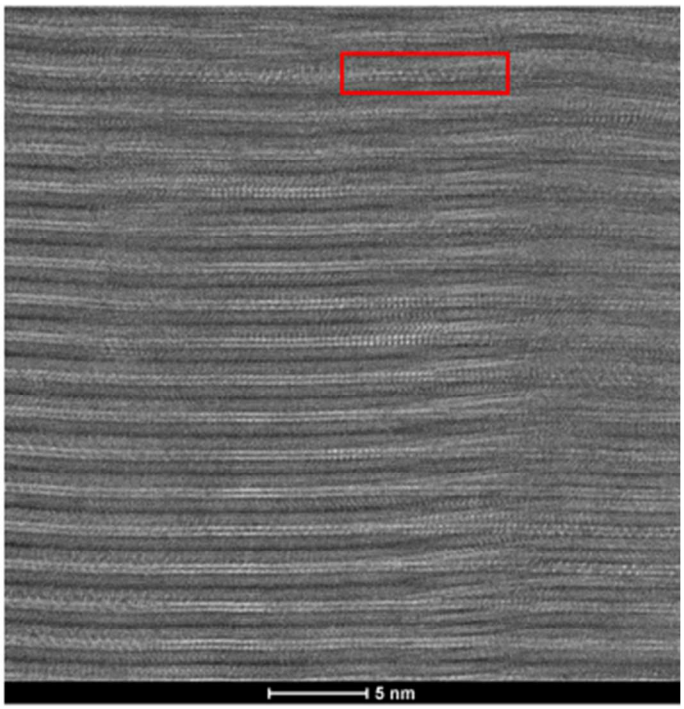

1,2: Image 22.07.07

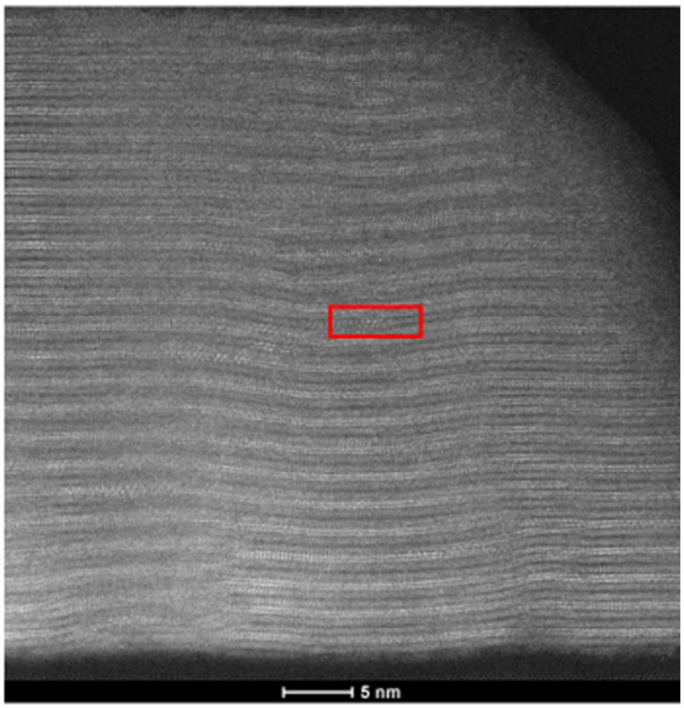

1,2: Image 22.08.36

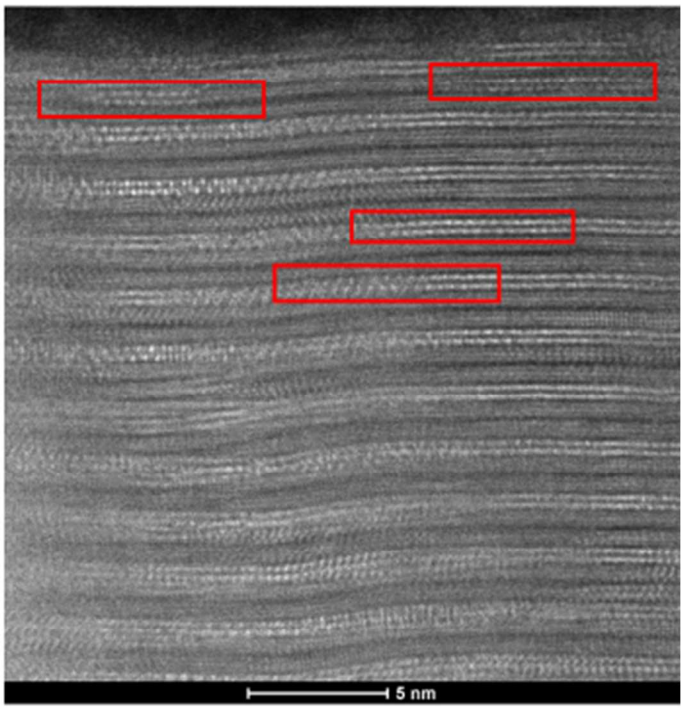

1,3: Image 09.55.37

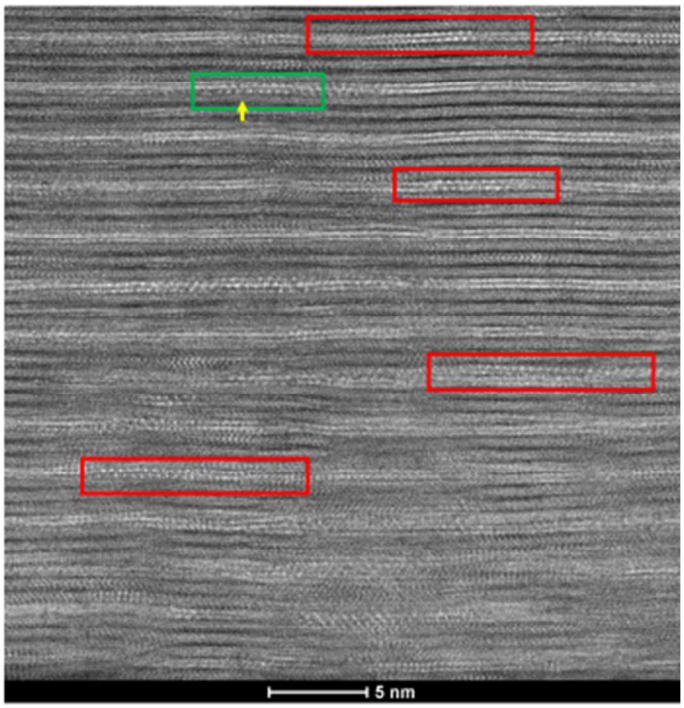

1,3: Image 09.57.09

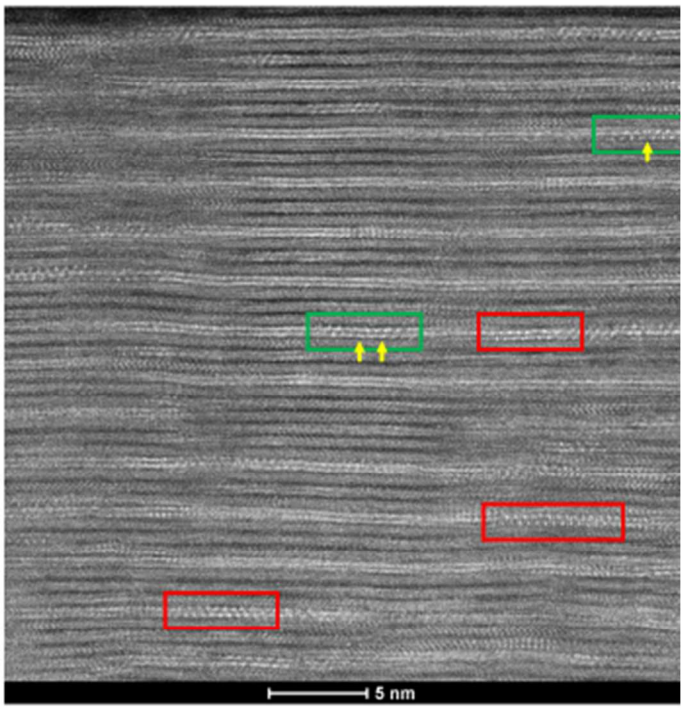

1,3: Image 09.58.05

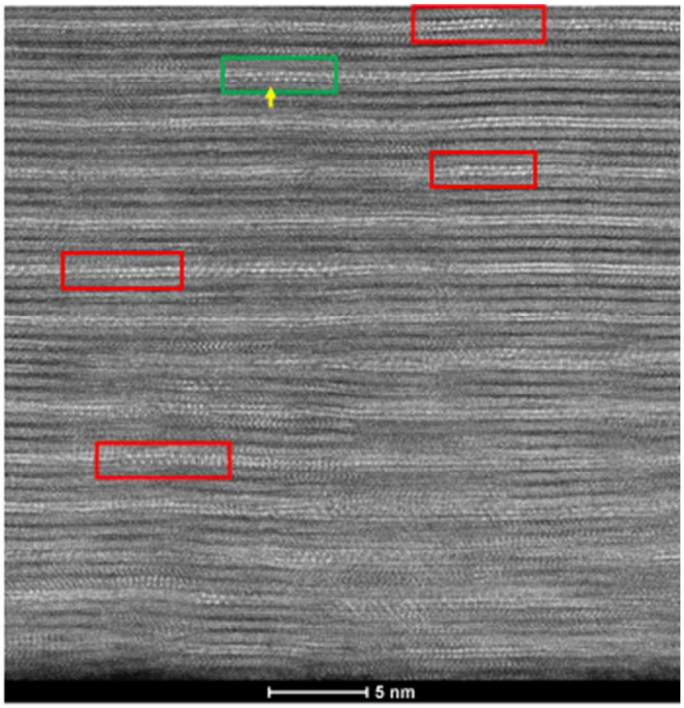

1,3: Image 10.01.05

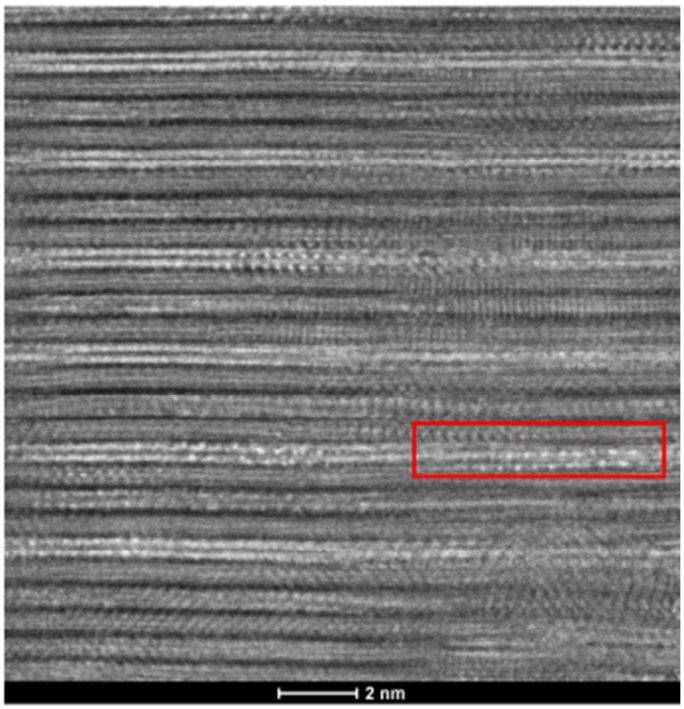

1,3: Image 10.03.16_000

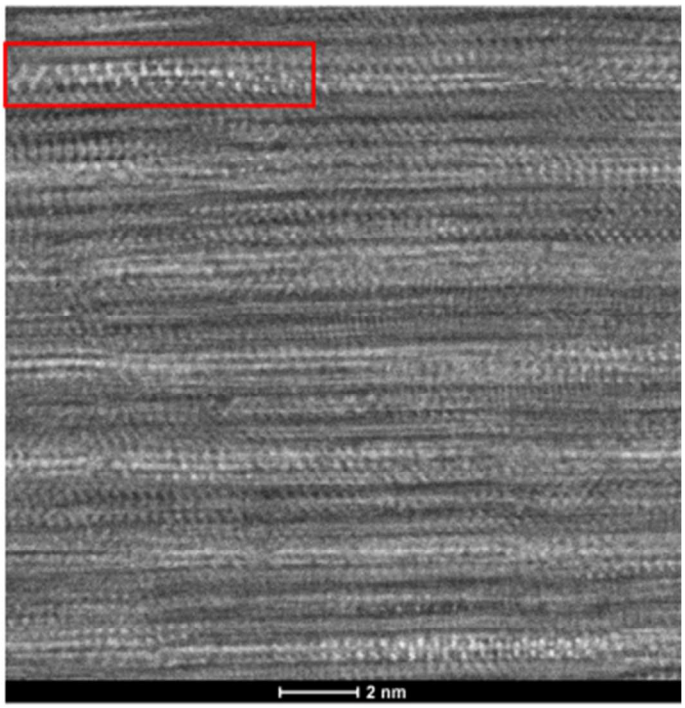

1,3: Image 10.03.16_001

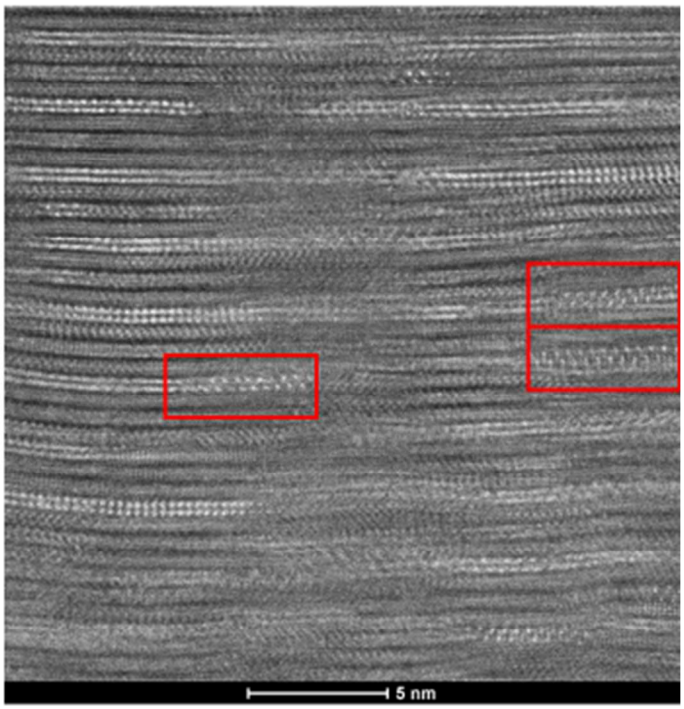

1,3: Image 10.03.16_003

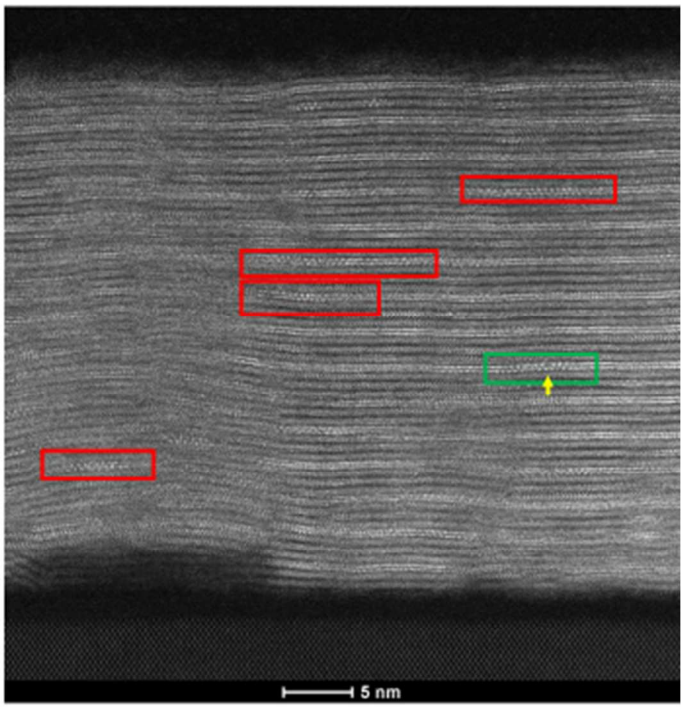

1,3: Image 10.03.16_005

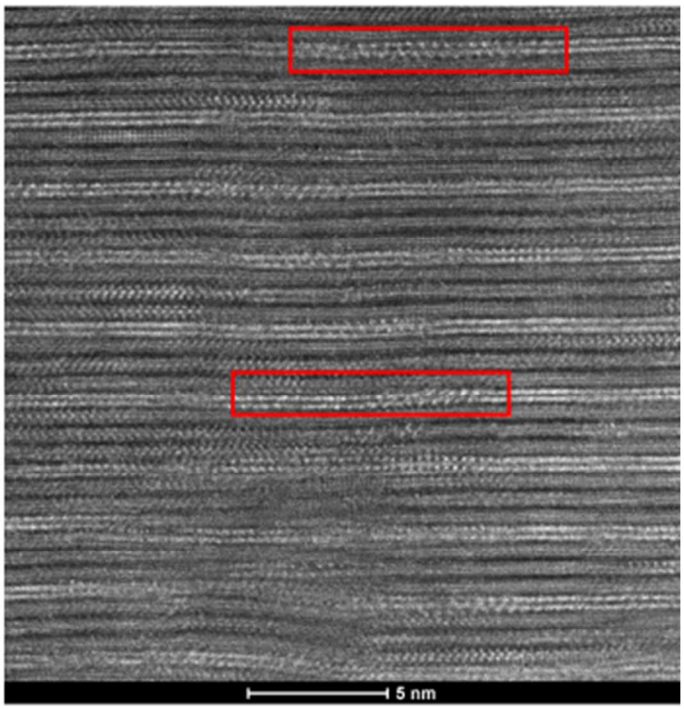

1,3: Image 10.08.23

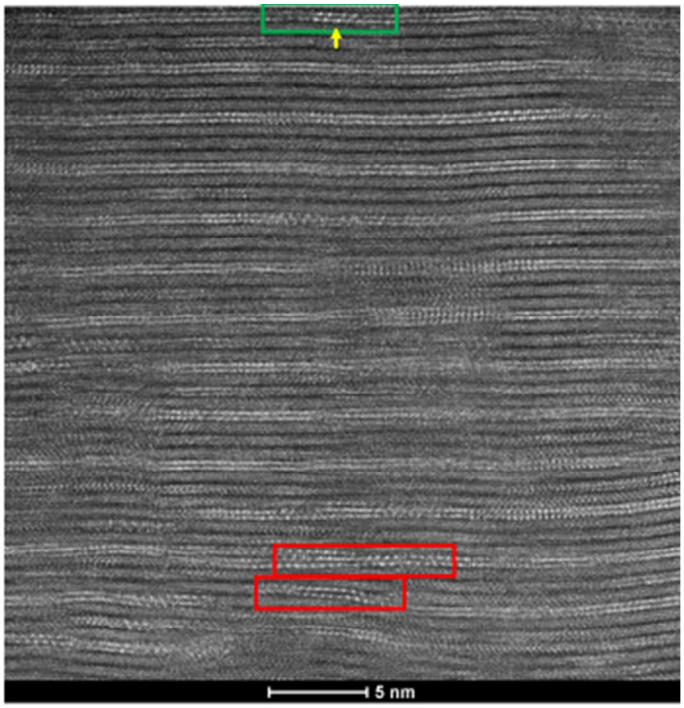

1,3: Image 10.11.04

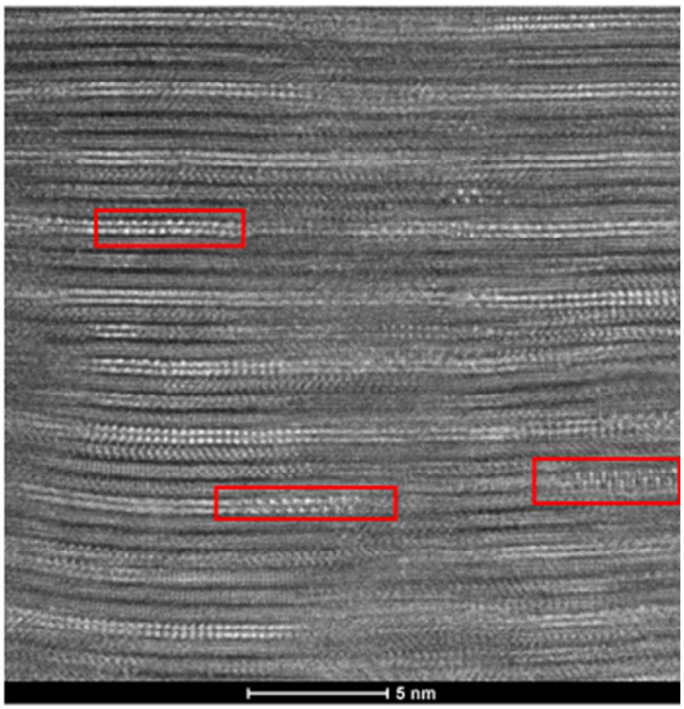

1,3: Image 10.12.41

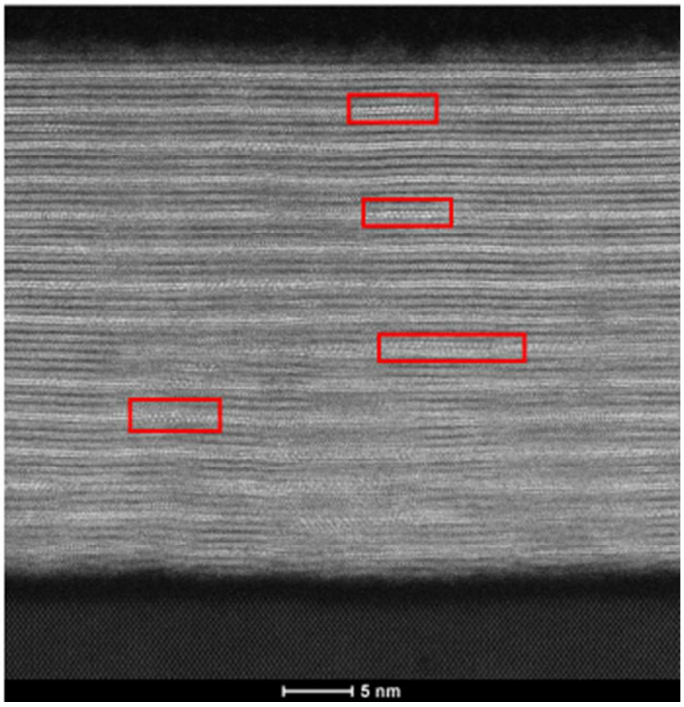

1,3: Image 10.13.27

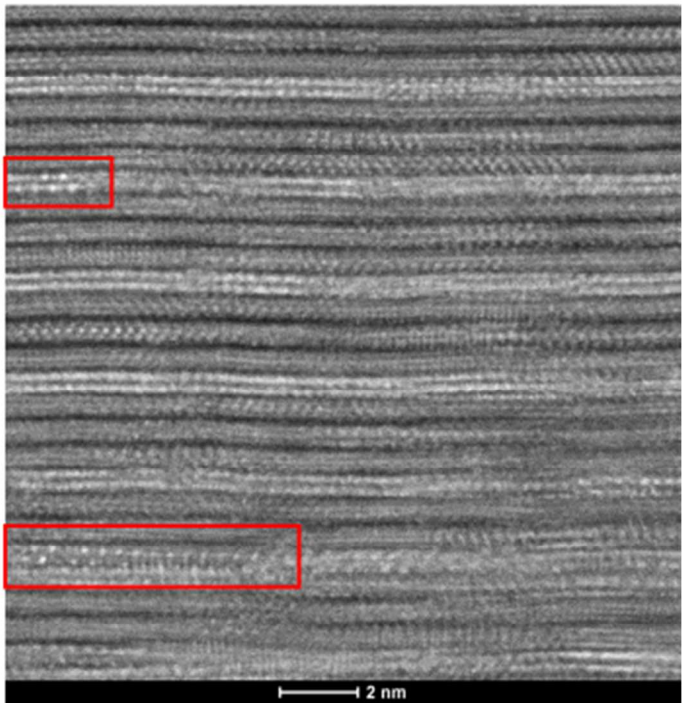

1,4: Image 21.10.57

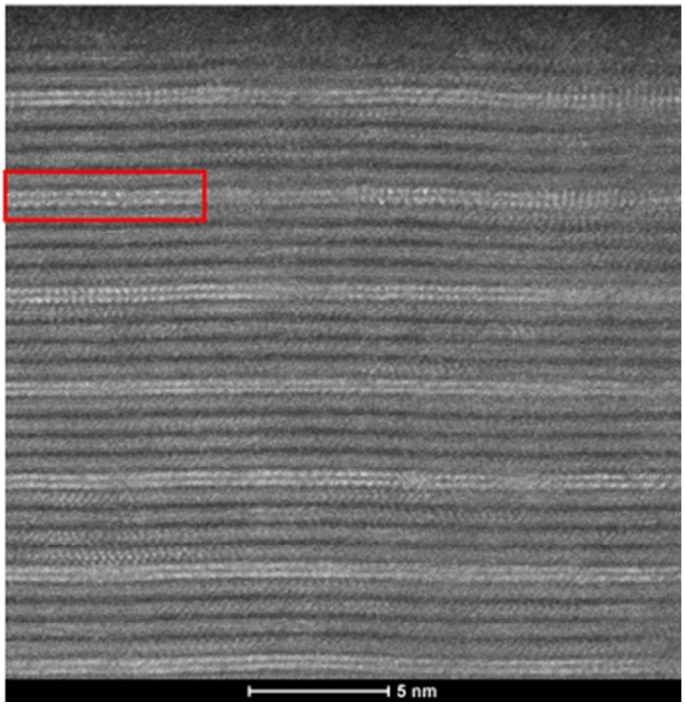

1,4: Image 21.13.17

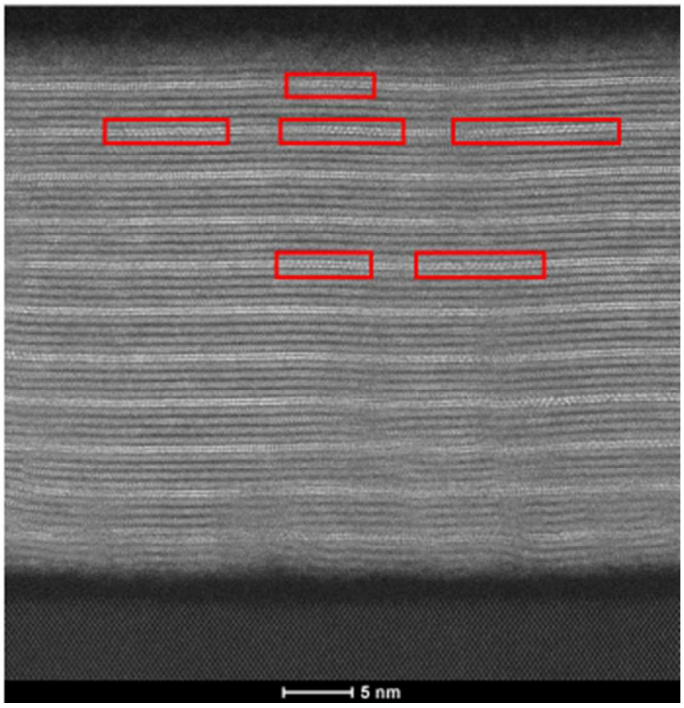

1,4: Image 21.14.28

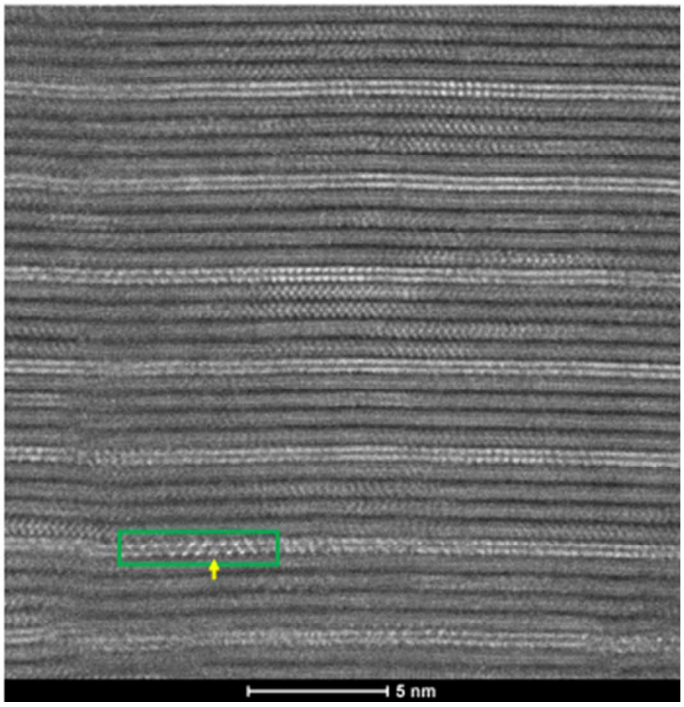

1,4: Image 21.15.28

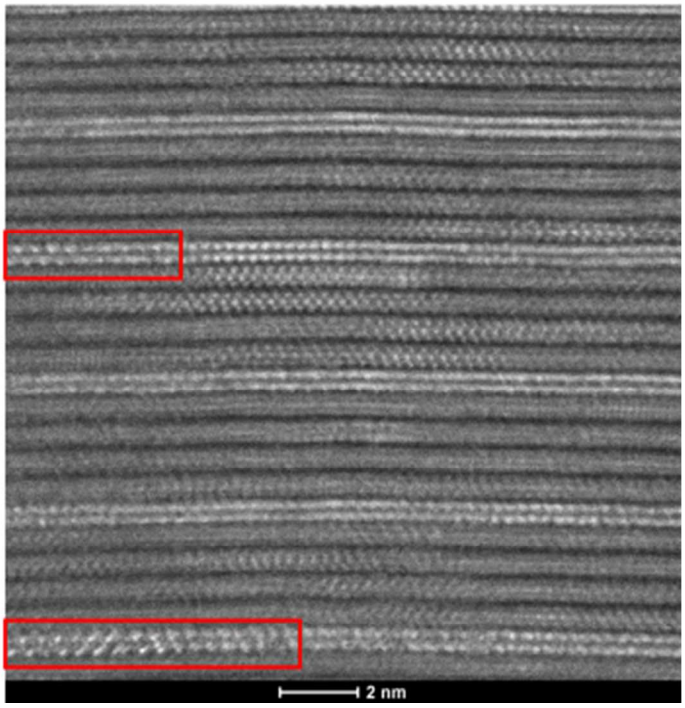

1,4: Image 21.17.39

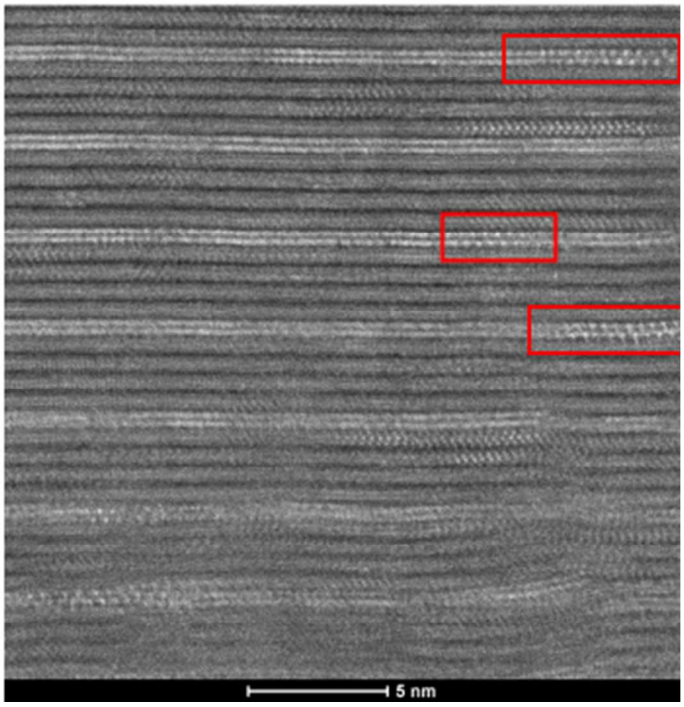

1,4: Image 21.19.23

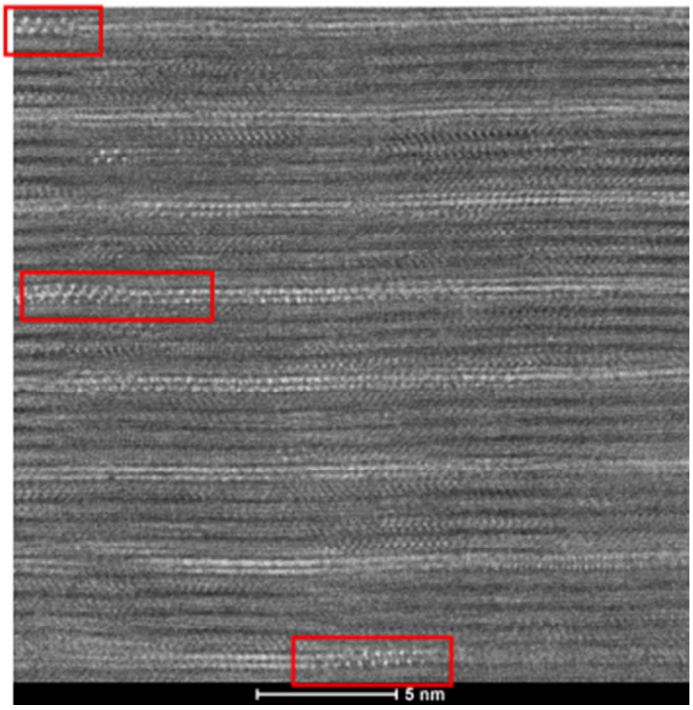

1,4: Image 21.20.22

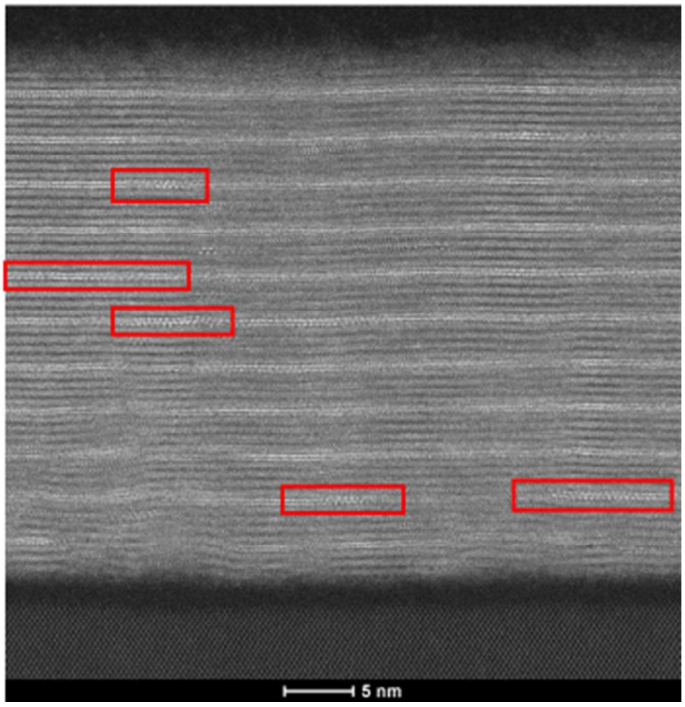

1,4: Image 21.23.32

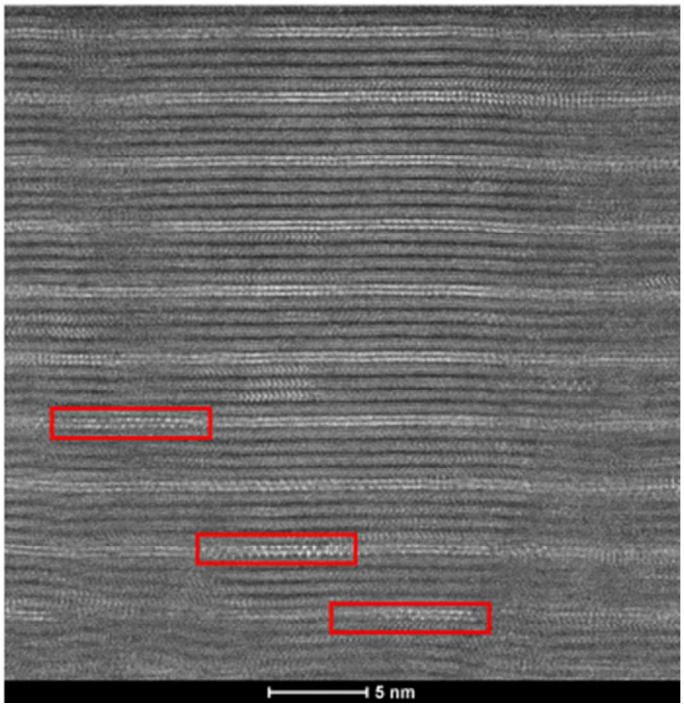

1,4: Image 21.24.30

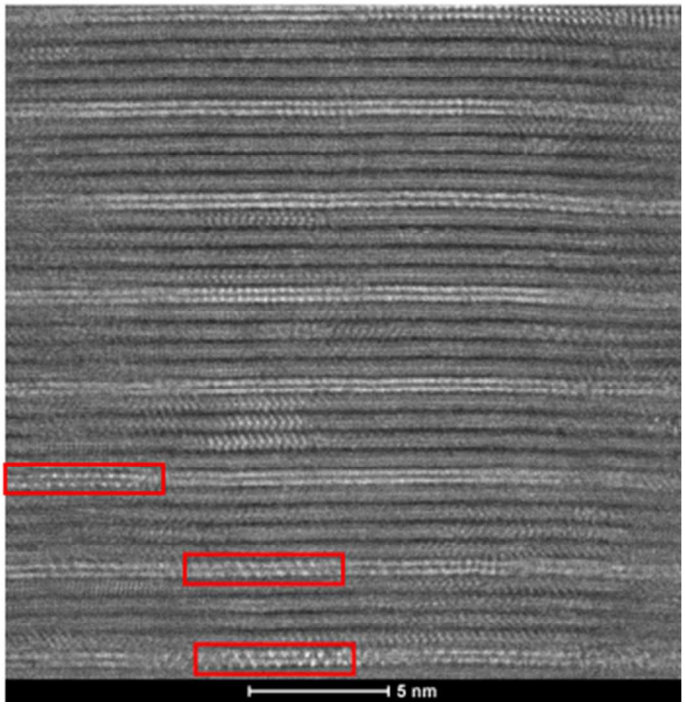

1,4: Image 21.27.44

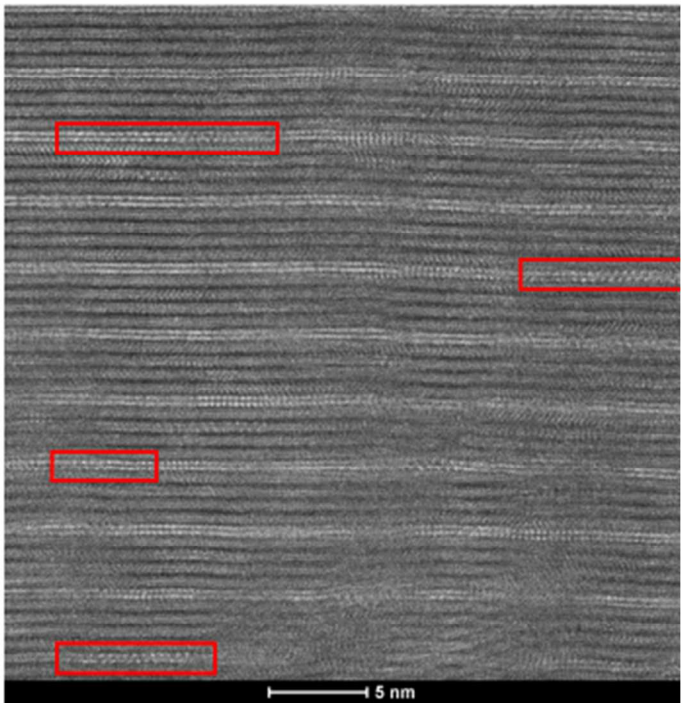

1,4: Image 21.29.18

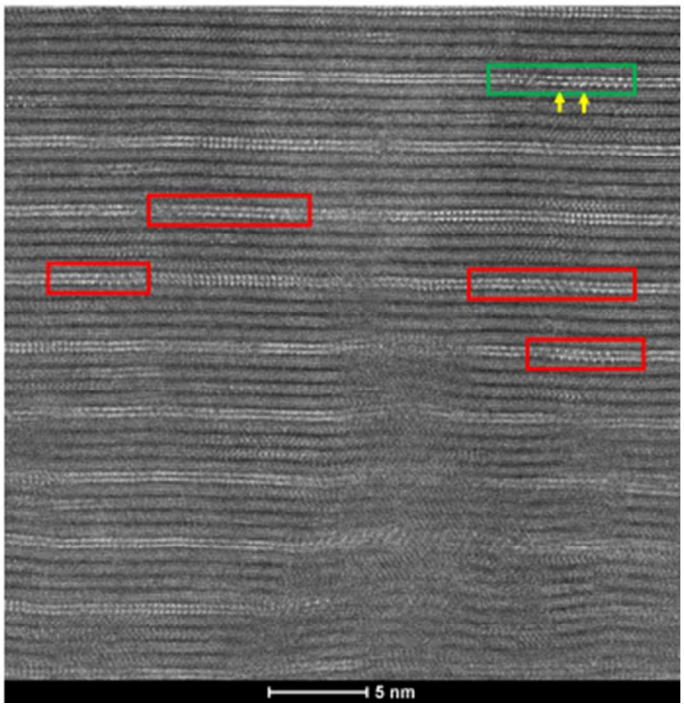

1,4: Image 21.33.10